Transmission Electron Scattering (TEM) Microscopy, X-Ray Diffractometer, and Raman Spectroscopy

Mugale Yogesh Gopal¹ & Suryawanshi Venkat S.²

^{1,2}Department of Chemistry, P.G. and Research Centre, Shri Chhatrapati Shivaji College, Omerga. Corresponding Author: yogeshmugale1991@gmail.com

Abstract: Zinc ferrite (ZnFe₂O₄) nanoparticles possess remarkable magnetic and catalytic properties, making them ideal candidates for applications in energy, electronics, and environmental remediation. This study presents a comparative analysis of ZnFe₂O₄ nanoparticles synthesized using two distinct methods: conventional combustion and microwave-assisted combustion. The synthesized samples were thoroughly characterized using XRD, FTIR, HR-SEM, TEM, UV-Vis spectroscopy, PL spectroscopy, BET surface area analysis, and VSM measurements. Both synthesis routes successfully yielded nanostructured ZnFe₂O₄ with a cubic spinel phase. However, the microwave method led to smaller crystallite sizes, increased surface area, and enhanced saturation magnetization compared to the conventional approach. SEM and TEM revealed that microwave combustion promoted the formation of well-defined nanorods and reduced agglomeration. Optical studies showed band gap variations attributable to morphological and structural differences. Catalytic activity was evaluated via the oxidation of alcohols using H₂O₂ as a green oxidant. Microwave-synthesized ZnFe₂O₄ displayed superior catalytic performance due to its higher surface area and active site density. This work underscores the significance of synthesis technique in tuning the physicochemical properties of ferrite nanomaterials and offers insights into designing efficient catalysts through advanced combustion strategies.

Keywords: Magnetic Nanoparticles, Iron Oxide Nanoparticles, Superparamagnetism, Biomedical and Environmental Applications.

1. Introduction

Nanoscience, a frontier of modern research, encompasses the study and application of materials at the nanoscale—typically less than 100 nanometers in at least one dimension. Nanotechnology, the applied facet of this field, has revolutionized various domains such as medicine, electronics, environmental science, and materials engineering. Among the myriad of nanostructured materials, magnetic nanoparticles (MNPs) stand out due to their unique size-dependent magnetic, thermal, and structural properties. These characteristics, along with their surface modifiability and functional versatility, make MNPs highly attractive for interdisciplinary applications, ranging from biomedical imaging and drug delivery to catalysis and environmental remediation.

The defining feature of MNPs lies in their superparamagnetic behavior when reduced below a critical size, typically around 15–20 nm. Unlike bulk ferromagnetic materials, these particles exhibit magnetism only under an external magnetic field, losing residual magnetism when the field is removed. This makes them highly suitable for biomedical applications, such as targeted drug delivery, magnetic resonance imaging (MRI), hyperthermia treatment of cancer, and bioseparation, where controlled magnetic responsiveness is crucial. The superparamagnetic nature also reduces magnetic dipole interactions, enhancing colloidal stability and biocompatibility in physiological environments.

Iron oxide-based nanoparticles, particularly magnetite (Fe₃O₄) and maghemite (γ -Fe₂O₃), are among the most commonly explored MNPs due to their biocompatibility, chemical stability, and ease of synthesis. These particles are widely employed in both in vivo and in vitro biomedical systems. Their applications span from MRI contrast agents to biosensors and drug

carriers, facilitated by their functional surfaces which can be engineered with polymers, ligands, or bioactive molecules to improve stability, targeting, and circulation time in biological systems.

The synthesis method profoundly influences the morphology, size distribution, crystallinity, magnetic behavior, and surface chemistry of nanoparticles. Conventional techniques such as co-precipitation, sol-gel processing, hydrothermal synthesis, microemulsion, and laser ablation each offer distinct advantages and limitations in terms of scalability, environmental impact, and control over particle characteristics. For example, co-precipitation is favored for its simplicity and efficiency in producing large quantities of iron oxide nanoparticles, though it may lack precision in size uniformity. The sol-gel technique, on the other hand, provides better control over chemical composition and homogeneity but often involves longer processing times and organic solvents.

Recent advances in green chemistry and nanobiotechnology have also introduced biological synthesis routes using plant extracts or microbial cultures. While these methods are environmentally benign and cost-effective, they still pose challenges in terms of reproducibility and monodispersity of the final product. Regardless of the method, the ability to tailor the size, surface functionality, and magnetic properties of MNPs is critical to optimizing their performance for specific applications.

Surface modification plays a pivotal role in enhancing the stability, dispersibility, and functionality of MNPs. Encapsulation in biocompatible polymers such as dextran, polyethylene glycol (PEG), chitosan, or polyvinyl alcohol (PVA) shields the particles from oxidation and aggregation, while allowing for the conjugation of targeting ligands, fluorescent dyes, or therapeutic agents. These tailored nanoparticles can then be directed to specific tissues or organs using external magnetic fields, thereby improving the efficacy of therapeutic or diagnostic procedures while minimizing off-target effects.

Moreover, the integration of MNPs with advanced materials like reduced graphene oxide (rGO), silica, or other metal oxides further expands their applicability. Such composites exhibit enhanced thermal stability, surface area, and magnetic tunability, enabling multifunctional platforms for simultaneous imaging, therapy, and sensing. These hybrid nanomaterials also find use in environmental applications, such as wastewater treatment, where magnetic separability and catalytic activity are critical.

Despite significant progress, several challenges remain. Ensuring consistent batch-to-batch synthesis, achieving precise size and shape control, and understanding the long-term biocompatibility and toxicity profiles of MNPs are ongoing research priorities. Additionally, regulatory and manufacturing hurdles need to be addressed for clinical translation and commercial deployment of MNP-based technologies.

This study aims to explore the synthesis, structural and magnetic characterization, and potential applications of iron oxide nanoparticles prepared via sol-gel and co-precipitation methods. Emphasis is placed on analyzing the effects of synthesis parameters on particle morphology, crystalline structure, thermal stability, and superparamagnetic behavior. The nanoparticles are characterized using a suite of techniques, including X-ray diffraction (XRD), scanning and transmission electron microscopy (SEM and TEM), Fourier transform infrared spectroscopy (FTIR), thermogravimetric analysis (TGA), vibrating sample magnetometry (VSM), and Mössbauer spectroscopy.

Furthermore, the incorporation of reduced graphene oxide with nickel-zinc ferrite nanoparticles is examined to evaluate the impact of hybridization on magnetic and thermal properties. The results provide critical insights into the structure—property relationships of MNPs and inform the rational design of multifunctional nanomaterials for biomedical and environmental use.

2. Literature survey:

Eirini Myrovali et al. (2021) explored how externally applied fixation fields enhance the collective magnetic properties of iron oxide nanoparticles by regulating dipolar interactions and promoting chain formation. Using coprecipitation, nanoparticles ranging from 10 to 80 nm were synthesized—both below and above the superparamagnetic limit of 25 nm. Under fixation fields of 40–400 mT, large particles formed chains via direct interactions, while smaller ones formed chains in two stages: clustering followed by cluster alignment. These arrangements intensified dipolar interactions, significantly improving magnetic response and hyperthermia efficiency. This study highlights how structuring nanoparticles into chains under controlled fields can enhance their performance in magnetic field-based applications.

Arbab Ali et al. (2021) reviewed the growing impact of magnetic nanoparticles (MNPs) across diverse fields such as healthcare, biosensing, agriculture, cancer theranostics, and environmental applications. Emphasizing the importance of surface engineering, the study outlines key synthesis methods and functionalization techniques essential for tailoring MNPs for specific uses. It highlights their roles as imaging agents, biosensors, and drug delivery vehicles. The review also addresses current limitations, offers mechanistic insights, and discusses future prospects for MNPs in advancing technology and biomedical innovations, providing a comprehensive overview of their synthesis, applications, and potential.

Kalpeshkumar S. Wagh et al. (2023) highlighted the significant potential of magnetic nanoparticles (MNPs) in therapeutic applications. Advances in nanoscale material synthesis and modification have enabled the development of clinically relevant MNPs with tailored properties. characteristics—such as superparamagnetism, Key high coercivity, biocompatibility, non-toxicity, and low Curie temperature—make them suitable for diverse biomedical uses. Their physico-chemical properties influence pharmacokinetics and cellular interactions. Clinically, MNPs are mainly applied in targeted drug delivery, magnetic hyperthermia, and as contrast agents in magnetic resonance imaging (MRI). Essential factors include morphology, hydrodynamic size, surface charge, and compatibility, which collectively enhance their effectiveness and safety in medical treatments.

Jonas Schwan et al. (2023) emphasized the importance of stability in various physiological fluids for the effective application of magnetic iron oxide nanoparticles (MIONs) in both in vitro and in vivo environments. Nanoparticles must remain stable during transitions from storage media to biological environments like blood or cell culture fluids. Using magnetosomes from magnetotactic bacteria as biogenic models, the study examined the colloidal stability of commercially available nanoparticles with different surface coatings. Stability was evaluated using dynamic light scattering, specifically the average intensity-weighted particle size (z-value), which also indicates protein corona formation—an important factor in biomedical applications.

Amarjeet Bisla et al. (2022) noted that since Feynman's iconic statement in the 1950s,

nanotechnology has rapidly advanced, impacting fields like medicine and veterinary science. In reproductive biology, particularly spermatozoa research, nanoparticles are increasingly used for semen cryopreservation, fertility evaluation, sperm imaging, gene transfer, and antioxidant delivery. However, the growing industrial application of magnetic and metallic nanoparticles has raised concerns about their potential toxic effects on male germ cells in humans and animals. This study explores both the beneficial applications and toxicological impacts of metallic nanoparticles on mammalian spermatozoa.

Pratishtha Kushwaha et al. (2023) demonstrated a simple one-step sol-gel synthesis of α - and γ -Fe₂O₃ nanoparticles without requiring costly reagents, pH adjustments, or controlled environments. Structural and morphological analyses were conducted using XRD, FE-SEM, HR-TEM, and EDX, confirming particle sizes of approximately 18.37 nm (α -Fe₂O₃) and 11.47 nm (γ -Fe₂O₃). FT-IR spectroscopy identified iron oxide and water-related stretching vibrations. VSM analysis showed weak magnetic properties, with a saturation magnetization of ~0.725 emu/g, remanence of 0.095 emu/g, and coercivity around 100.26 Oe. The nanoparticles were spherical and composed solely of iron and oxygen, indicating their potential for magnetic applications.

Yu R. Mukhortova et al. (2022) developed a Fe₃O₄/rGO biocomposite with promising biomedical applications, including MRI, drug delivery, and magnetic therapy. Magnetite nanoparticles (MNPs) were synthesized via co-precipitation, followed by citric acid (CA) functionalization and adsorption onto rGO sheets. MNPs formed in an inert atmosphere showed enhanced phase purity and reduced size. CA reduced agglomeration without altering structure. Magnetization measurements under a pulsed magnetic field (up to 6.5 kOe) showed the highest saturation magnetization (80.27 emu/g) in MNPs prepared without CA. In vitro tests identified optimal MNP concentrations to minimize cytotoxicity. Future work will explore magnetic field effects on cellular response in polymer composites.

Ryan Hufschmid et al. (2018) investigated the influence of nanoscale chemical and magnetic structures on iron oxide nanoparticles for magnetic particle imaging (MPI) using Mössbauer spectroscopy and EELS. Two 27 nm nanoparticle samples—one optimized with oxidation, one not—were analyzed. Optimized particles formed single-crystalline magnetite (Fe₃O₄), ideal for MPI, while unoptimized ones exhibited an antiferromagnetic wüstite (FeO) phase, unsuitable for MPI. Mössbauer data showed optimized nanoparticles were 70% magnetite and 30% maghemite; unoptimized were 60% magnetite and 40% wüstite. EELS-STEM analysis confirmed phase and crystallographic consistency in optimized particles and revealed coreshell structures in mixed-phase samples due to interfacial spin interactions.

Sahar I.A. Al-Baldawi et al. (2019) explored the synthesis and characterization of magnetite (Fe₃O₄) nanoparticles using co-precipitation, a standard method involving a 1:2 molar ratio of ferrous to ferric ions in basic solutions. The synthesized nanoparticles exhibited an average size of 11 ± 2 nm via dynamic light scattering and 13 ± 2 nm via TEM analysis. These methods revealed spherical, well-dispersed nanoparticles. At pH 6.5 ± 0.1 , the zeta potential measured -24 ± 2 mV, attributed to citric acid's carboxylic groups on the surface. This negative potential prevents aggregation, ensuring nanoparticle stability and dispersion in colloidal systems.

Magnetic nanoparticles (MNPs) have emerged as transformative tools across disciplines due to their unique magnetic properties and nanoscale behavior. Eirini Myrovali et al. (2021) investigated how external fixation fields can enhance dipolar interactions, enabling the

formation of chain-like architectures of iron oxide nanoparticles. Particles above 25 nm easily form chains through particle-particle interactions, while smaller ones require clustering, followed by chain formation. This alignment significantly improves magnetic hyperthermia efficiency.

Arbab Ali et al. (2021) reviewed the synthesis, functionalization, and applications of MNPs across fields like cancer theranostics, biosensing, and agriculture. Engineering surface characteristics is critical to unlocking their full potential, including use as imaging agents and drug carriers.

Kalpeshkumar S. Wagh et al. (2023) emphasized MNPs' therapeutic potential, attributing it to properties such as superparamagnetism, biocompatibility, and low toxicity. Their effectiveness in drug delivery, magnetic hyperthermia, and MRI contrast enhancement is closely tied to morphology, surface charge, and hydrodynamic size.

Jonas Schwan et al. (2023) focused on the importance of MNP stability in physiological media. The study compared various coatings and measured colloidal stability using dynamic light scattering and zeta potential, helping to predict nanoparticle performance and protein corona formation.

Amarjeet Bisla et al. (2022) explored the role of nanoparticles in semen biology, highlighting applications in cryopreservation, fertility assessment, and sperm-mediated gene transfer. As industrial use rises, evaluating both the toxic and beneficial effects of metallic MNPs on mammalian spermatozoa becomes crucial for safe application in veterinary and human medicine.

Pratishtha Kushwaha et al. (2023) synthesized α - and γ -Fe₂O₃ nanoparticles using a simple one-step sol-gel method without costly reagents or complex controls. Characterization through XRD, FE-SEM, and HR-TEM confirmed spherical nanoparticles of about 18.37 nm (α) and 11.47 nm (γ) sizes. FT-IR revealed iron oxide and water functional groups, while magnetic studies showed low saturation magnetization (\sim 0.725 emu/g) and coercivity (\sim 100 Oe).

Yu R. Mukhortova et al. (2022) developed Fe₃O₄/reduced graphene oxide (rGO) biocomposites for biomedical applications like MRI and targeted therapy. Magnetite nanoparticles were synthesized via co-precipitation, citric acid functionalization, and rGO adsorption. Synthesizing in inert conditions improved phase purity and reduced particle size. Magnetic measurements showed high saturation magnetization (up to 80.27 emu/g) and reduced agglomeration after citric acid addition. Biological tests optimized safe MNP concentrations for cell applications.

Jhelai Sahadevan et al. (2021) produced Fe₂O₃ and Fe₃O₄ nanoparticles by solvothermal synthesis using ferric nitrate with ethylene and diethylene glycol. Fe₃O₄ formed cubic particles (~15.16 nm) with ferromagnetic behavior, while Fe₂O₃ had rhombohedral structure (~31.22 nm) and superparamagnetic properties confirmed by magnetic analysis.

Lenuța Crintea et al. (2020) synthesized magnetite and maghemite nanoparticles via coprecipitation for industrial wastewater treatment, effectively degrading organic dyes like methylene blue under UV light. Characterization included SEM, XRD, UV-Vis, and magnetic circular dichroism. Ryan Hufschmid et al. (2018) studied 27 nm iron oxide nanoparticles using Mössbauer and electron energy loss spectroscopy, revealing that optimized oxidation yields mainly magnetite and maghemite phases suitable for magnetic particle imaging, while unoptimized particles contain unwanted wüstite. Shoeb Anwar Mohammed Khawja Ansari et al. (2018) reviewed synthesis, functionalization, and biomedical applications of iron oxide nanoparticles (IONPs), emphasizing their magnetic properties for brain and spinal cord disorder treatments. Kamil Gareev et al. (2022) discussed biomimetic nanomaterials mimicking natural structures for applications like bioimaging, targeted therapy, and hyperthermia. Ayad Mohammed et al. (2024) provided an overview of Fe₂O₃ nanoparticle synthesis methods and their diverse applications in medicine, electronics, catalysis, and sensing.

Shalini Rajput et al. (2024) characterized chemically co-precipitated Fe₃O₄ nanoparticles using techniques like VSM, XRD, TEM, and FT-IR. These nanoparticles effectively removed Cr⁶⁺ and Pb²⁺ from water, with optimal adsorption at pH 2.0 for Cr⁶⁺ and pH 5.0 for Pb²⁺. Adsorption followed pseudo-second-order kinetics and fit best with the Langmuir and Sips isotherm models. Maximum adsorption capacities were 34.87 mg/g for Cr6+ and 53.11 mg/g for Pb²⁺ at 45°C. The nanoparticles also showed good reusability for wastewater treatment.

Magnetite nanoparticles (MNPs) have attracted significant interest across various fields, especially biomedicine, due to their unique magnetic, physico-chemical, and surface functionalization properties. Recent advances focus on optimized synthesis methods, surface coatings, and multifunctional applications such as targeted drug delivery, imaging, and diagnostics.

Andrea Paut et al. (2024) developed a microwave hydrothermal synthesis of magnetite nanoparticles using chamomile flower extract as a natural reducing and stabilizing agent. This eco-friendly one-precursor method yielded superparamagnetic magnetite NPs with distinct properties compared to traditional methods. Characterization techniques such as FTIR, PXRD, SEM, and magnetometry confirmed their structure and magnetic behavior. Notably, these coated particles exhibited selective cytotoxicity against cancer cells, indicating their potential for biomedical use.

Similarly, Fahima Dilnawaz et al. (2022) emphasized the promise of magnetic nanoparticles in nanomedicine for drug delivery, diagnostics, and imaging, highlighting the importance of superparamagnetism and biocompatible polymer coatings to enhance multifunctionality. K. Prem Ananth et al. (2013) demonstrated that microwave irradiation can control magnetite nanoparticle size (27–40 nm), influencing magnetic properties vital for biomedical applications.

Biological synthesis methods offer eco-friendly alternatives to chemical and physical approaches. Nadeem Joudeh et al. (2022) reviewed biogenic nanoparticles synthesized via microorganisms or plants, emphasizing their unique physical and chemical properties and wide applications across electronics, agriculture, and healthcare. This bio-oriented approach allows scalable, sustainable production while retaining desirable nanoparticle features.

Gabriela Fabiola Stiufiuc et al. (2024) summarized the biomedical relevance of magnetic nanoparticles, focusing on biofunctionalization techniques, precise control over size, shape, and surface area, and characterization methods crucial for tailoring magnetic properties to specific applications.

Justine Wallyn et al. (2019) detailed the development of superparamagnetic iron oxide nanoparticles (SPIONs) for multifunctional biomedical roles including drug delivery, imaging, and real-time monitoring, leveraging their customizable architectures for enhanced targeting and therapeutic effects.

Additional research by Anuvansh Sharma et al. (2021) introduced DNA-encapsulated iron oxide nanoparticles as innovative, environmentally safe tracers for hydrological monitoring, showcasing the versatility of MNPs beyond medicine. Arbab Ali et al. (2021) reviewed the broad spectrum of MNP applications spanning agriculture, medicine, biosensing, and catalysis, stressing the critical role of surface engineering to achieve multifunctionality. Lastly, studies such as those by Alina Mihaela Prodan (2013) and Attarad Ali et al. (2015) reinforced the biocompatibility, antibacterial activity, and therapeutic potential of iron oxide nanoparticles, while highlighting advances in synthesis, characterization, and clinical prospects. Collectively, these works underscore magnetite nanoparticles as a rapidly evolving platform with diverse applications driven by innovative synthesis, functionalization, and characterization strategies.

3. Methodology:

This section offers a clear summary of the fundamental principles underlying each characterization technique used in the study. It also outlines the specific models, instrument configurations, and experimental conditions applied, including key parameters such as operating range, resolution, temperature, and other essential specifications relevant to accurate data collection and analysis.

3.1. Diffractometer for X-Rays:

X-ray diffraction (XRD) is a vital technique for determining the structural properties of crystalline materials, such as unit cell parameters and crystallite size. It operates on the principle that X-rays are diffracted by crystal planes with interplanar spacings (\sim 2–3 Å) comparable to the X-ray wavelength. This diffraction follows Bragg's law: $2d\sin\theta = n\lambda$, where d is the interplanar spacing, θ is the diffraction angle, and λ is the X-ray wavelength. In this study, measurements were performed using a Bruker D8 diffractometer with Cu–K α radiation ($\lambda = 1.5418$ Å), scanning from 10° to 80° . The crystallite size (D) was estimated using the Debye–Scherrer equation: $D = k\lambda / \beta \cos\theta$, where k is a shape factor (typically \sim 0.93–0.94), β is the full width at half maximum (FWHM) of the peak, and θ is the Bragg angle. For detailed analysis of lattice parameters and grain size, Rietveld refinement was conducted using MAUD software. Figure 1 shows Schematic illustration of Bragg's diffraction law.

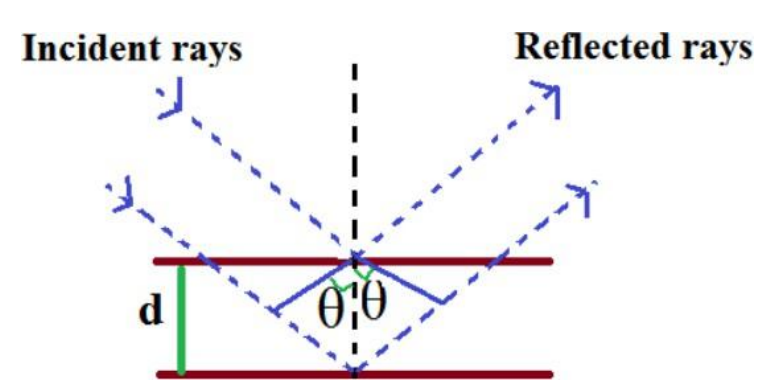


Figure 1. Schematic illustration of Bragg's diffraction law

3.2. FESEM, or scan electron microscope that uses field emission technology:

Field Emission Scanning Electron Microscopy (FESEM) is widely used to investigate the

surface topography of materials at high resolution. In this technique, a focused beam of high-energy electrons emitted from a field emission gun is directed onto the sample surface. The interaction between the incident electrons and the sample generates various signals, which are collected to produce detailed surface images. In this study, surface morphology was examined using an Inspect FEI microscope (USA), which provided high-resolution imaging of the samples. Figure 2 presents a schematic illustration of the fundamental working principle of FESEM.

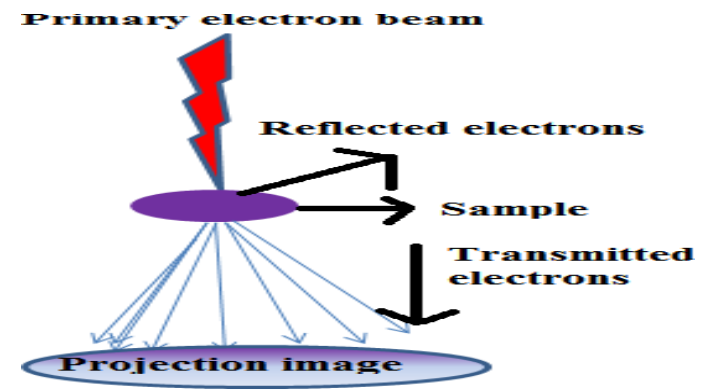


Figure 2. Schematic representation of basic principle of FESEM

3.3. Microscope for Transmission Electron Scattering (TEM)

Transmission Electron Microscopy (TEM) is a powerful technique used to analyze the morphology of materials at the nanoscale. In this method, a highly energetic electron beam is transmitted through an ultra-thin specimen, interacting with its internal structures. The resulting transmitted electrons are captured using imaging systems such as digital detectors or fluorescent screens, producing high-resolution images. High-Resolution TEM (HRTEM) allows for visualization at the atomic scale, offering exceptional structural detail. Complementary techniques like Selected Area Electron Diffraction (SAED) and Energy Dispersive X-ray (EDX) spectroscopy are often employed alongside TEM for crystallographic and elemental analysis. In this study, a JEOL JEM-2011 instrument was used to acquire detailed TEM images. Figure 3 shows TEM's schematic depiction of its operating principle.

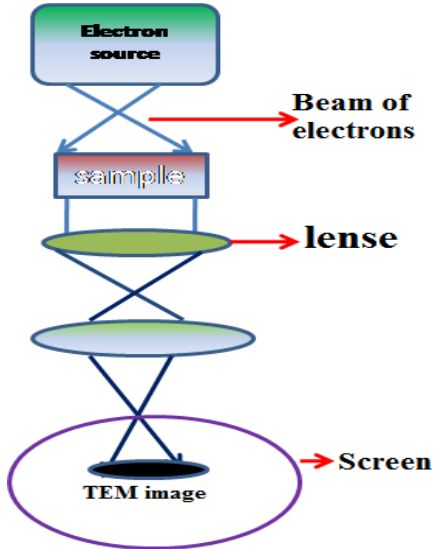


Figure 3. TEM's schematic depiction of its operating principle

3.4. Examinations conducted with the use of HR-TEM microscopy:

High-Resolution Transmission Electron Microscopy (HRTEM) was employed to analyze the microstructure, morphology, and thermal effects on the samples. Imaging and Selected Area Electron Diffraction (SAED) patterns were obtained using a Philips CM20 Super Twin microscope, operating at 200 kV with a 300 keV electron beam. Sample preparation involved grinding the materials with a mortar and pestle, followed by ultrasonic dispersion in methanol. A drop of the resulting suspension was deposited onto a perforated carbon-coated copper grid, ensuring appropriate sample thickness and stability for effective HRTEM observation.

3.5. Application of Thermogravimetric Analysis:

Thermogravimetric Analysis (TGA) is a key technique for assessing thermal stability by monitoring a sample's mass change as a function of temperature over time. It provides insights into physical phenomena such as phase transitions, adsorption, and desorption, as well as chemical reactions like decomposition and chemisorption. During the analysis, the sample is gradually heated in a controlled environment until specific thermal events occur. The results are plotted as a TGA curve, with mass loss (as a percentage of the initial mass) on the y-axis and temperature or time on the x-axis. In this study, selected samples were examined using a TA Instruments SDT-Q600, heated from room temperature to 800°C at a rate of 10°C/min under a nitrogen atmosphere.

3.6. Imaging in the Infrared Range (FTIR):

Fourier Transform Infrared (FTIR) spectroscopy is a powerful analytical method used to identify chemical bonds and functional groups, particularly in organic compounds. Molecules absorb infrared radiation at characteristic frequencies that correspond to specific vibrational modes of their chemical bonds. The resulting absorption spectrum serves as a molecular fingerprint, revealing the types of functional groups present in the sample. In this study, detailed FTIR spectra were obtained using a JASCO FTIR-460 instrument to facilitate comprehensive chemical analysis. Figure 4 illustrates the fundamental principle of FTIR spectroscopy.

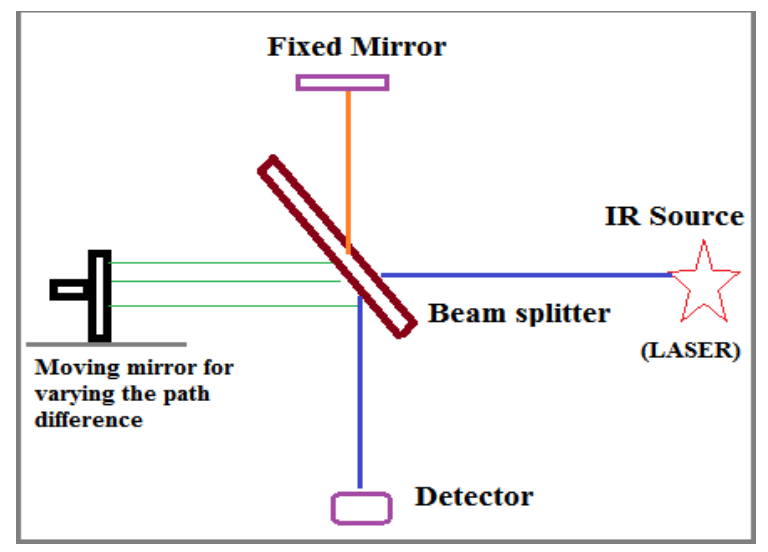


Figure 4. Fundamental concept of FTIR

3.7. Small-Angle Energy-Dispersive X-Ray Fluorescence:

Energy Dispersive X-ray Fluorescence (ED-XRF) is widely employed to assess the elemental composition and purity of samples. In this technique, elements within the sample are simultaneously excited, prompting the emission of characteristic X-rays unique to each element. These emissions are detected by an energy-dispersive detector linked to a multichannel analyzer, which distinguishes and quantifies the elemental signatures based on their energy levels. For this study, ED-XRF analysis was performed using the EX-3600 system from M-S Jordan Valley, Israel, while micro-EDXRF measurements were conducted with the XGT-7200 instrument from Horiba Scientific.

3.8. Raman Spectroscopy:

Raman spectroscopy is a powerful tool used to explore lattice distortions, structural transitions, spin—lattice and charge—lattice interactions, magnetic ordering, and the local distribution of cations within materials. The technique operates on the principle of inelastic scattering of monochromatic light, typically from a laser source. As the laser light interacts with molecular vibrations or phonons in the sample, the scattered photons exhibit a shift in energy. This energy shift reveals detailed information about the material's vibrational modes. In this study, Raman spectra were acquired using the LabRAM HR Raman spectrometer from Horiba.

3.9. Spectroscopy that uses both visible and ultraviolet light:

By using ultraviolet light spectroscopy, one may identify the materials optical bandgap. Valence electrons of the outermost layer of valence band absorb light and gets excited to conduction band. That particular excitation wavelength resembles width of the material's band. Using Tauc plot, $(\alpha h v) = A (h v - Eg)^n$, hv be the incident energy, α , the coefficient of absorption, Where n is the number of nanometers in the band gap and Eg is a constant. = $\frac{1}{2}$ or 2 for the band gap may be determined by calculating the materials direct or indirect transitions. Across all available experiments here JASCO 530V UV-VIS spectrophotometer was used.

3.10. Photocatalytic Activity:

The photocatalytic performance of the material was evaluated using organic dyes as probe molecules, specifically methylene blue and rhodamine B, under visible light exposure. A 200 W tungsten lamp ($\lambda \ge 410$ nm) served as the light source, with a 1 M NaNO₂ solution acting as a UV cutoff filter. Dye solutions at a concentration of 10^{-5} M were prepared and stirred continuously for 30 minutes using a magnetic stirrer to achieve adsorption-desorption equilibrium before testing.

3.11. Mossbauer Spectroscopy:

Mössbauer spectroscopy is a highly sensitive technique that analyzes gamma-ray absorption and emission in solids to detect minute changes in nuclear energy levels influenced by the local atomic environment. It provides insights into key interactions such as isomer shift, quadrupole splitting, and hyperfine splitting. The method achieves exceptionally high energy resolution—on the order of parts per 10^{11} —by relying on recoil-free (resonant) gamma-ray absorption and emission, ensuring conservation of momentum. In this study, transmission-mode Mössbauer

spectroscopy was carried out at room temperature (300 K) using a WissEl GmbH spectrometer equipped with a 512-channel PC-based analyzer. Calibration was performed using a 12 μ m thick natural iron foil. The isomer shift (δ) indicates variations in nuclear resonance energy due to electron density changes in the s orbital, while quadrupole splitting provides information on the interaction between nuclear energy levels and the surrounding electric field gradient.

3.12. Dielectric property:

An HP LCR meter (Model 4284A) was used to characterize the processed samples. The capacitance of the parallel-plate capacitor system was calculated using the equation $C=\epsilon'\epsilon 0A/d$, where $\epsilon 0$ is the vacuum permittivity, A is the surface area of the pellet, and d is the thickness. Pellets were prepared with a diameter of 13 mm and a thickness of 1 mm using the synthesized powder. Silver paste was applied on both surfaces to ensure ohmic contact. The dielectric permittivity (ϵ) was determined using the relation ϵ =Cd/ $\epsilon 0A$.

3.13. Squid magnetometer:

Low magnetic moment detection is achieved using a SQUID (Superconducting Quantum Interference Device), which exploits quantum interference effects in superconductors combined with a low coercive field to deliver exceptional sensitivity. The device consists of superconducting loops with Josephson junctions and can detect magnetic fields as weak as 5 × 10⁻¹⁸ T. There are two primary types of SQUID magnetometers: direct current (DC) and radio frequency (RF). In this study, magnetic measurements were performed using a Quantum Design MPMS XL-7 system at various temperatures, including room temperature (300 K) and low temperatures (10 K and 5 K). Samples were subjected to external magnetic fields, causing magnetic dipoles to align with the applied field. The magnetization versus applied field relationship is depicted by the M–H loop (magnetic hysteresis curve), from which key magnetic parameters—such as saturation magnetization (Ms), coercivity (Hc), remanent magnetization (Mr), and magnetic anisotropy constant (K1)—were determined.

3.14. VSM Measurements:

In this experiment, the magnetic response of the samples was measured using a PMC MicroMag 3900 vibrating sample magnetometer (VSM) with a 1 Tesla magnet. An external magnetic field ranging from -10,000 to +10,000 Oe was applied, and all measurements were carried out at room temperature without cooling the samples.

4. Results and Discussions:

4.1. Comparative Methods Of Synthesis, CharacterizationAnd Catalytic Oxidation Of Alcohols By Zinc Ferrite (ZnFe₂O₄) Nanoparticles Through Conventional And Microwave Method:

Creating functional nanostructures that combine excellent properties with reliable fabrication methods remains a key challenge in materials science. Recently, inorganic nanocrystals have attracted considerable research interest due to their unique low-dimensional properties and wide-ranging technological applications. Among these, ferrites—magnetic ceramic oxides mainly composed of ferric ions—stand out for their heat and corrosion resistance, affordability, and usability at high frequencies, despite having lower saturation magnetization than ferromagnetic alloys. Spinel ferrite nanoparticles, with the general formula AB₂O₄ where A

and B represent divalent and trivalent cations respectively, have gained attention for potential applications in biomedicine and other fields. Zinc ferrite (ZnFe₂O₄) is particularly notable because its crystal structure maintains the coordination of Zn²⁺ ions at tetrahedral sites and Fe³⁺ ions at octahedral sites, influencing its magnetic behavior.

Developing synthesis methods that produce nanosized zinc ferrite with enhanced magnetic properties compared to bulk material is therefore desirable. Bulk ZnFe₂O₄ exhibits typical zinc ion placement in its spinel structure, but its nanoscale form opens up opportunities for improved functional performance. Zinc ferrite is economically important and has diverse uses, including gas sensors, catalysts, photocatalysts, absorbents, information storage devices, and electronics. Microwave-assisted combustion synthesis offers significant advantages over traditional heating methods. Unlike conventional approaches where heat is transferred externally, microwaves directly interact with the sample to generate heat internally, leading to faster synthesis times, improved reaction kinetics, and better phase control. This technique stabilizes metastable phases by energy transfer from microwave fields, allowing precise control over chemical processes' kinetic and thermodynamic factors.

Selective oxidation of alcohols is critical in organic synthesis and chemical industries, where environmentally friendly oxidants like hydrogen peroxide (H₂O₂) are preferred over harmful stoichiometric oxidants. H₂O₂ is safe, inexpensive, and decomposes into water and oxygen, making it ideal for green oxidation processes when paired with metal oxide catalysts.

This study presents a novel, cost-effective, and straightforward microwave combustion method for synthesizing ZnFe₂O₄ nanoparticles with tunable size and morphology, exhibiting promising catalytic activity, offering a more efficient alternative to conventional combustion techniques.

4.2. Findings and Analysis:

4.2.1. Investigation using XRD or X-ray scattering:

Figure 5 presents the XRD analysis of ZnFe₂O₄ samples A and B synthesized via the microwave combustion technique. The diffraction patterns clearly exhibit the crystalline nature of the ZnFe₂O₄ ferrites, showing characteristic peaks corresponding to the spinel structure's main planes: (220), (311), (400), (422), (511), and (440), consistent with the single-phase cubic spinel structure (JCPDS card no. 22-1012). All peaks were indexed to the cubic Fd3m space group, confirming the formation of a pure spinel phase without impurities. The samples displayed high crystallinity and were synthesized under identical conditions, ensuring reproducibility. Crystallite sizes were calculated using the Scherrer formula applied to the most intense peak, with values of 23.45 nm for sample A and 21.89 nm for sample B. These results support the idea that microwave combustion produces smaller, more uniformly distributed crystallites due to its lower combustion exothermicity compared to conventional methods, resulting in improved control over particle size and phase purity.

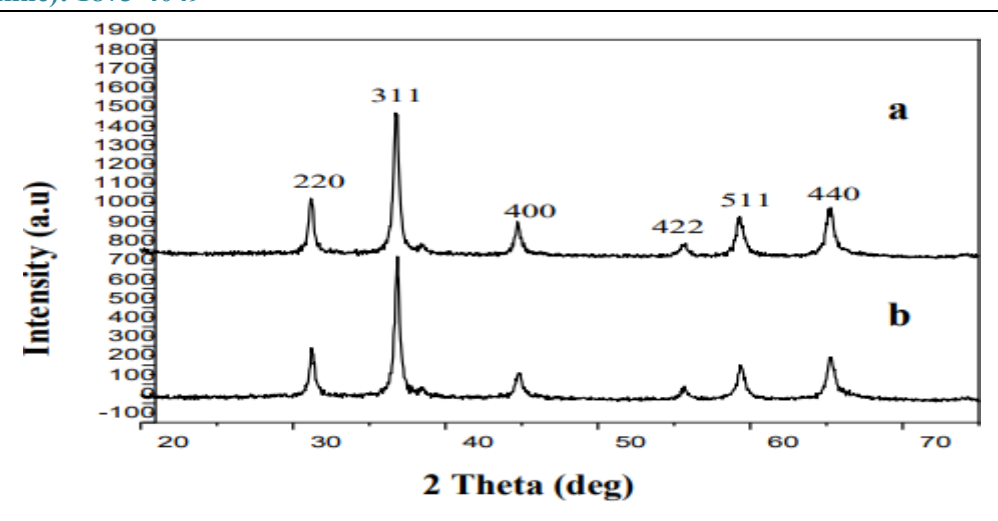


Figure 5. Pattern of XRD for Zinc ferrite samples (A and B)

4.2.2. Examination using FT-IR spectra Fourier transform:

The FT-IR spectra of the ZnFe₂O₄ samples, shown in Figure 6 (a-b), provide further structural insights. A broad band around 3450 cm⁻¹ corresponds to –OH stretching vibrations from hydroxyl groups involved in hydrogen bonding. An absorption near 1600 cm⁻¹ is attributed to water molecule deformation, likely from moisture absorbed during powder compaction. Both samples exhibit a peak around 1500 cm⁻¹, linked to Fe–O bond vibrations. Metal–oxygen stretching vibrations (M–O, Fe–O, and M–O–Fe) appear prominently between 400 and 1000 cm⁻¹. The region from 2000 to 950 cm⁻¹ shows deformation modes of Fe–OH and Zn–OH bonds, with strong multiple bands indicating –OH deformation. Weak bands between 2380–2360 cm⁻¹ and 2090–2040 cm⁻¹ suggest carbonate ions from atmospheric CO₂. No impurity phases are detected, consistent with XRD results, confirming the typical cubic spinel structure.

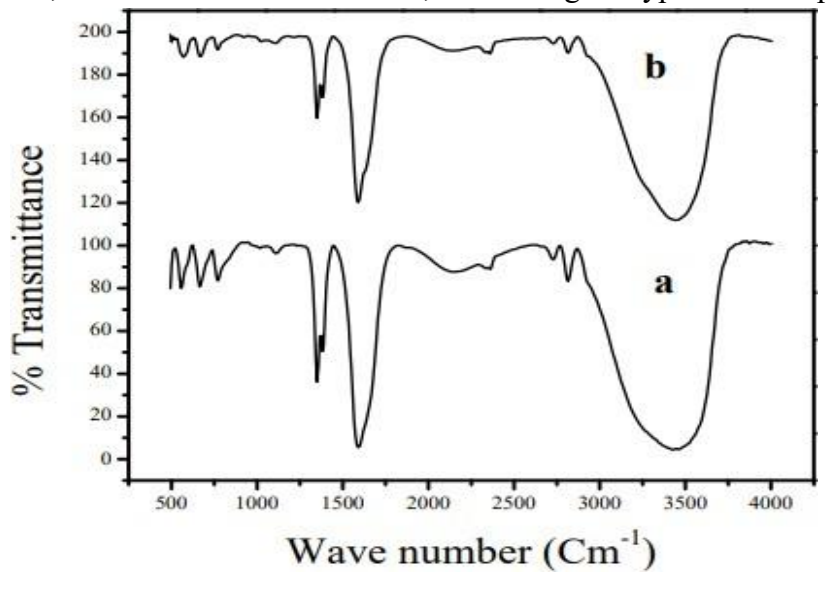


Figure 6. FT-IR analysis of two zinc ferrite samples

4.2.3. Examinations using HR-SEM

The morphology of the synthesized zinc ferrite was examined using high-resolution scanning electron microscopy (HR-SEM). Structural and morphological characteristics are essential for practical applications. The chemical synthesis method used produces ZnFe₂O₄ particles with shapes and sizes comparable to those obtained via traditional and microwave-assisted L-arginine-nitrate methods. SEM images reveal a mixture of nanorod and spherical particles with varied sizes distributed throughout the samples.

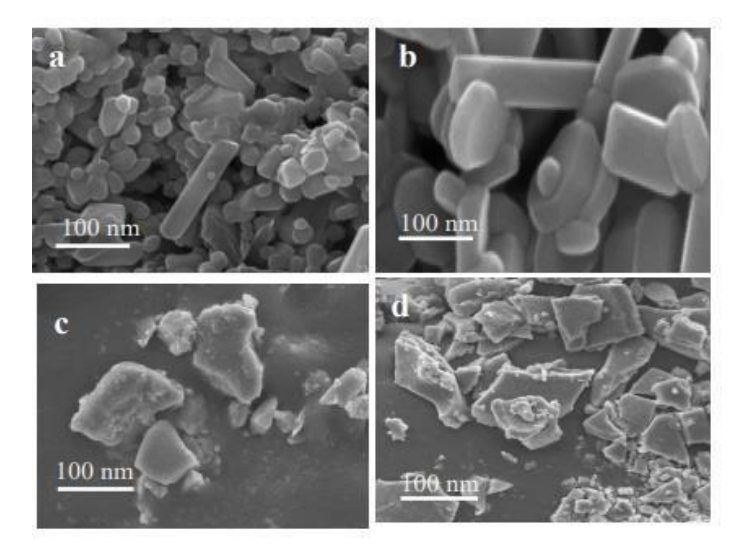


Figure 7. HR-SEM pictures of ZnFe2O4 sample A (a, b) and sample B (c, d) made using the traditional and microwave methods, respectively

Short ZnFe₂O₄ nanorods (Figure 7 (c, d)) are prominently formed in Sample B, prepared via microwave combustion, whereas they appear rarely in Sample A (Figure 7 (a, b)). The significant increase in gaseous byproducts during combustion leads to the formation of highly porous, voluminous powders, with their characteristics depending on the fuel used. Sample A, containing glycine, exhibits a higher concentration of octahedral nanorods compared to Sample B, which uses L-arginine. Furthermore, Sample B shows noticeable nanoparticle agglomeration, unlike Sample A. According to XRD data, Sample A has a slightly more compact crystallite size than Sample B. The difference between particle sizes measured by XRD and SEM is minimal. This discrepancy arises because XRD calculates crystallite size based on coherently diffracting crystal domains, while SEM and TEM observe grain boundaries visible through crystal contrast. As a result, XRD typically reports smaller sizes due to its stricter criteria.

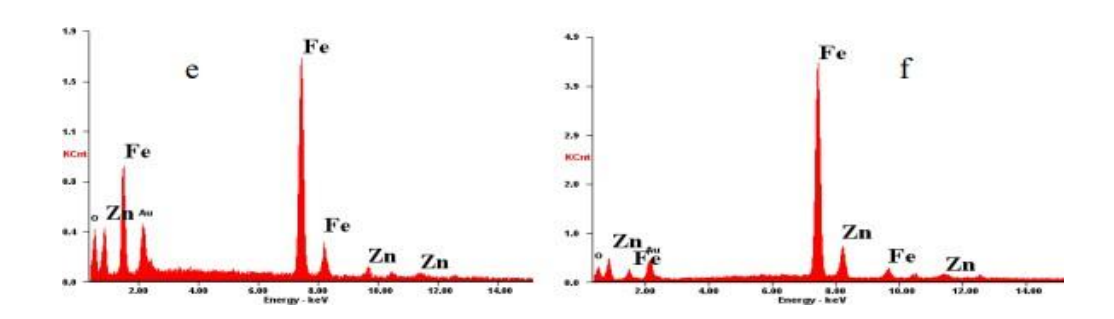


Figure 7 (e,f) EDX spectra of Zinc ferrite samples A and B

The presence of pure ZnFe₂O₄ was confirmed using Energy Dispersive X-ray Spectroscopy (EDX), as shown in Figure 7 (e, f). The EDX spectra clearly display characteristic peaks for Zn, Fe, and O, indicating the formation of ZnFe₂O₄. Additionally, the samples were coated with gold prior to HR-SEM imaging, which resulted in the appearance of gold peaks around 2.1–2.2 keV in the spectra.

4.2.4. Research using transmission electron microscopy:

Transmission Electron Microscopy (TEM) was used to examine the structure and morphology of the samples. Both nanorods and nanoparticles were observed to be uniformly distributed, as shown in Figure 8 (a, b). Figure 8 (a) presents a clear image of the nanorods found in sample A. In contrast, particle aggregation was evident during the synthesis of sample B, as illustrated in Figure 8 (b). These results clearly demonstrate that the shape and structure of the nanopowders can significantly change depending on the type of fuel used in their preparation.

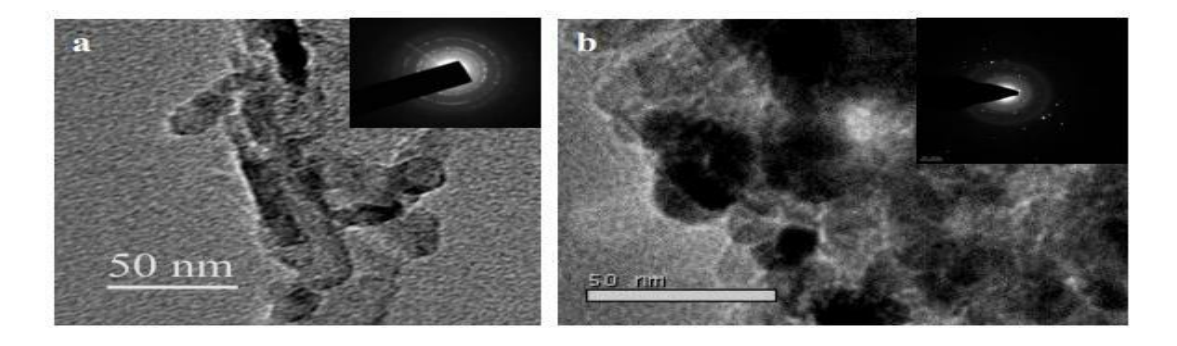


Figure 8. TEM pictures samples A and B of ZnFe₂O₄—(inset) - SAED pattern and related particles for ZnFe₂O₄

The slight discrepancy between particle sizes measured by XRD and HR-SEM can be attributed to factors such as structural disorder, lattice strain from varying ionic radii, and metal oxide clustering. It is inferred that L-arginine contributes to higher flame temperatures during synthesis, leading to particle agglomeration and a broader size distribution. In contrast, Sample A (glycine) produces moderately sized nanorods. Hence, the choice of fuel plays a crucial role

in determining the formation pathways, enabling the production of mixed morphologies including both nanorods and nanoparticles.

4.2.5. DRS analysis:

Figure 9 (a, b) presents the UV-Vis spectra of ZnFe₂O₄ samples A (glycine) and B (L-arginine) measured over the 200–800 nm range. All spectra exhibit a broad absorption band spanning 200–700 nm, with a prominent peak between 215 and 225 nm. Key insights from these spectra include information about spinel defects and the band gap energy. The high-energy peaks in ZnFe₂O₄ spinels correspond to electron transitions from occupied O 2p orbitals to vacant Fe 3s orbitals, potentially involving Fe 3p orbital mixing. Additionally, the broad shoulders observed at longer wavelengths are attributed to electronic transitions involving the filled O 2p and vacant Zn 4s orbitals, along with intrinsic spinel characteristics, particularly spinel-related defects.

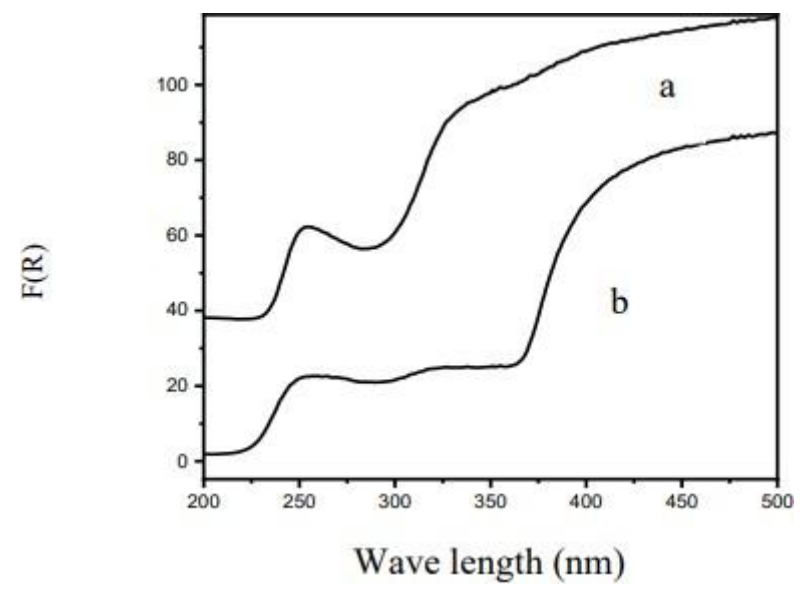


Figure 9. DRS spectra of ZnFe₂O₄ samples (A and B)

The Kubelka-Munk function, F(R)=(1-R)2/2R [24], can be used to relate the diffuse reflectance (R) of the samples, as shown in Figure 9. The prominent peak in the infrared and visible spectra of the synthesized metal oxides is attributed to primary band-to-band electron excitations. Additionally, a lower-energy absorption feature is observed, which is likely associated with spinel defects to varying degrees. The calculated band gap values range from 2.2 to 2.7 eV, reflecting the nanoscale size of the particles, and are notably higher than the 1.9 eV band gap typically found in bulk zinc ferrite.

4.2.6. PL Studies:

The photoluminescence (PL) spectrum was used to characterize samples A and B of ZnFe₂O₄. Figure 10 shows the room-temperature PL spectra, recorded with a scanning speed of 1000 nm/min. The ZnFe₂O₄ solution exhibited an emission maximum at 435 nm (with an excitation wavelength of 360 nm), while the solid form showed a blue-shifted emission. The emission spectra reveal an unusual distribution, indicating an inconsistent distribution of nanostructures.

Limited information is available on the PL behavior of ZnFe₂O₄ from previous studies. Structural defects such as Zn and O vacancies, likely caused by excess Zn and O ions, were observed in this experiment. The luminescence is attributed to these crystal structure defects, although the exact mechanism remains unclear.

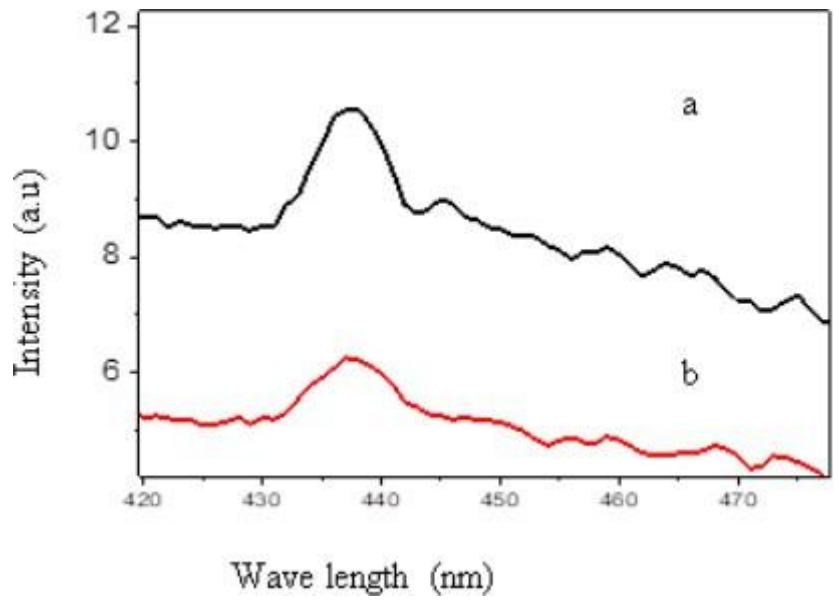


Figure 9. Two samples of ZnFe2O4 were examined by measuring their PL absorbance spectra at room temperature

ZnFe₂O₄ the decrease of oxygen vacancies and charge-compensating cation vacancies is to blame for this. Another piece of evidence supporting the band edge shift When the size of the particles changes, the changes in excitation and emission maxima.

4.3. Analyzing magnetic properties:

The key advantage of magnetic nanorods and nanoparticles lies in their ability to be controlled using an external magnetic field. The magnetic properties of samples A and B were measured at room temperature using a vibrating sample magnetometer (VSM) with an applied field up to 10 kOe, as shown in Figure 10. The figure also demonstrates that the samples can be effectively separated from water by applying an external magnetic field. Table 1 summarizes the saturation magnetization (Ms), remanent magnetization (Mr), and coercivity (Hc) values. The M-H hysteresis loops confirm that both samples exhibit ferromagnetic behavior with soft magnetic characteristics, which is influenced by magnetic anisotropy [29]. Sample A shows a higher saturation magnetization (Ms) of 30.08 emu/g compared to 22.86 emu/g for sample B. The ferromagnetism in ZnFe₂O₄ spinel arises from ion exchange and the compensation of sublattice magnetizations, resulting in net magnetization at tetrahedral and octahedral sites. Magnetic properties are highly sensitive to crystallinity, particle size, and morphology. Thus, sample A, synthesized using glycine, demonstrates superior magnetic performance in Ms, Hc, and Mr compared to sample B prepared with L-arginine.

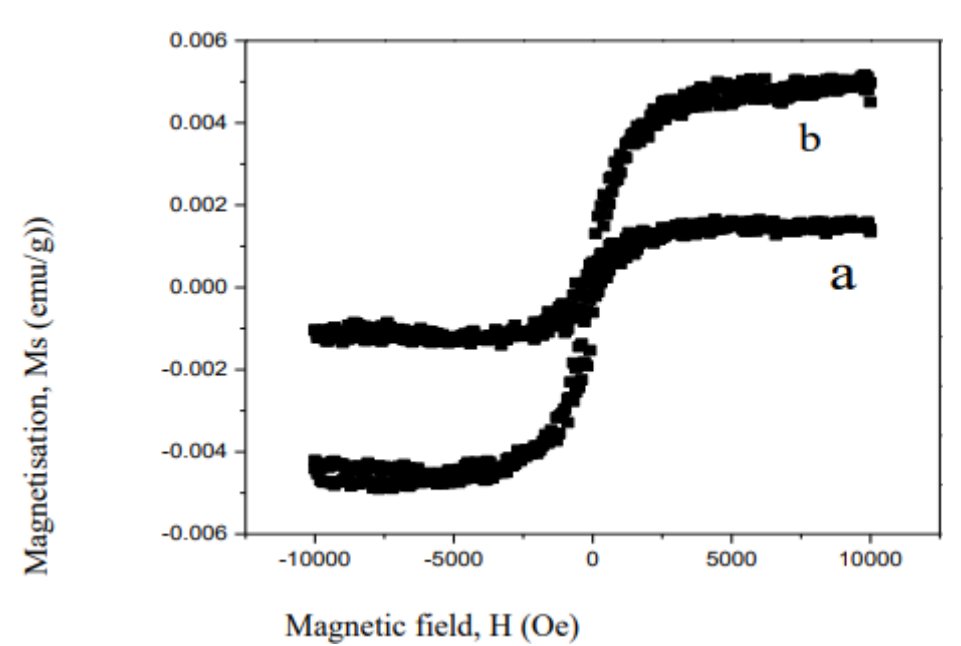


Figure 10. Samples A and B's magnetisation curves

Table 1. Information from VSMs of the ZnFe₂O₄ samples (A and B)

Sample	Coercivity (G)	Retentivity (emu/g)	Magnetization (emu/g)
Sample A	22.63	2.973	22.86
Sample B	30.23	4.1621	30.08

5.3.1. Research on porosity, surface area and volume:

By adding the appropriate amount of filler to zinc ferrite, its micropore volume and specific surface area can be enhanced without significantly changing the pore width. The specific surface area was determined by measuring nitrogen adsorption and applying the BET equation. The average micropore diameter was calculated using the H-K method, while the total pore volume and micropore volume were obtained from the t-plot analysis. The results, summarized in Table 2, provide a detailed view of the ZnFe₂O₄ nanostructures' pore characteristics based on BET analysis. The relatively large surface area of ZnFe₂O₄ promotes its catalytic activity by providing more active sites. The combination of high pore volume and surface area is particularly beneficial for catalysis. As expected, the surface area increases as particle size decreases. Nanostructures show a direct relationship between surface area, particle size, and defect density, which further enhances their suitability as catalyst supports.

Table 2. Variables such as Size of crystallites, average pore diameter, volume of pores, and BET surface area (in nanometres) and ZnFe2O4 prepared by microwave combustion method

ZnFe ₂ O ₄ Catalyst	Sample A	Sample B
SBET (m ² /g)	58.87	70.54
Rp (Å)	14.19	10.16
Vp (cm ³ /g)	0.0910	0.1191

5. Conclusion:

This study highlights the profound impact of synthesis methodology on the structural, morphological, magnetic, and catalytic properties of zinc ferrite (ZnFe₂O₄) nanoparticles. Two synthesis techniques—conventional combustion and microwave-assisted combustion—were employed to prepare ZnFe₂O₄ nanostructures. Comprehensive characterization revealed that both approaches successfully produced single-phase spinel structures. However, the microwave-assisted method resulted in finer crystallites, reduced particle agglomeration, and the formation of nanorods alongside spherical particles, as confirmed by HR-SEM and TEM imaging. XRD analysis demonstrated enhanced crystallinity and smaller particle sizes in microwave-synthesized samples, which also exhibited a higher BET surface area, thus providing more active sites for catalysis. Optical studies, including UV-Vis and PL spectroscopy, indicated a wider band gap in microwave-treated samples, reflecting the influence of quantum size effects and structural defects. Magnetic characterization using VSM revealed stronger ferromagnetic behavior and higher saturation magnetization in microwaveprepared ZnFe₂O₄, attributed to improved crystallinity and reduced surface disorder. Importantly, the microwave method significantly enhanced catalytic efficiency in the oxidation of alcohols using hydrogen peroxide, a green oxidant. This improvement is ascribed to the synergistic effect of increased surface area, porosity, and optimized morphology. Microwaveassisted synthesis proves to be a superior, energy-efficient, and scalable technique for tailoring ZnFe₂O₄ nanoparticles with desirable properties for environmental and catalytic applications. This study provides valuable insights for the development of next-generation ferrite-based nanomaterials and encourages further exploration into microwave processing for advanced functional nanomaterials.

References:

- 1. Kai Zhu, Yanmin Ju, Junjie Xu, Ziyu Yang, Song Gao, and Yanglong Hou Accounts of Chemical Research 2018 51 (2), 404-413 DOI: 10.1021/acs.accounts.7b00407
- 2. Alla Divya Naga Aparna, Dharamasoth Rama Devi, Keloth Basavaiah (2022) Magnetite Nanoparticles: Synthesis Methods A Comparative Review.
- 3. Alvarado-Noguez, Margarita L., Ana E. Matías-Reyes, Mario Pérez-González, Sergio A. Tomás, Claudia Hernández-Aguilar, Flavio A. Domínguez-Pacheco, Jesús A. Arenas-Alatorre, Alfredo Cruz-Orea, Mauricio D. Carbajal-Tinoco, Jairo Galot-Linaldi, and et al. 2023. "Processing and Physicochemical Properties of Magnetite Nanoparticles

- Coated with Curcuma longa L. Extract" Materials 16, no. 8: 3020. https://doi.org/10.3390/ma16083020
- 4. Che Soh, Siti & mohd yusof, Mohd & Abd Rahman Azmi, Alyza & Shamsuddin, Mustaffa & Wan Nor, Wan Fatihah. (2018). Synthesis and Physicochemical Properties of Magnetite Nanoparticles (Fe3O4) as Potential Solid Support for Homogeneous Catalysts. Malaysian Journal of Analytical Sciences. 22. 768-774. 10.17576/mjas-2018-2205-04.
- 5. Fadia, Saviska & Rahayu, Istie & Nawawi, Deded & Ismail, Rohmat & Prihatini, Esti & Laksono, Gilang & Wahyuningtyas, Irma. (2024). Magnetic characteristics of sengon wood-impregnated magnetite nanoparticles synthesized by the co-precipitation method. AIMS Materials Science. 11. 1-27. 10.3934/matersci.2024001.
- 6. Trifoi, Ancuta & Matei, Ecaterina & Râpă, Maria & Banu, Ionut & DOUKEH, Rami. (2023). Coprecipitation nanoarchitectonics for the synthesis of magnetite: a review of mechanism and characterization. Reaction Kinetics, Mechanisms and Catalysis. 136. 39. 10.1007/s11144-023-02514-9.
- 7. Devi, S. & Nivetha, Ambikapathi & Inbaraj, Prabha. (2019). Superparamagnetic Properties and Significant Applications of Iron Oxide Nanoparticles for Astonishing Efficacy—a Review. Journal of Superconductivity and Novel Magnetism. 32. 10.1007/s10948-018-4929-8.
- 8. Moniruz Zaman, Mohammad & Karal, Mohammad & Khan, Mohammed & Tareq, Abu Rayhan & Ahammed, Shareef & Akter, Mahmuda & Hossain, Aslam & Ullah, A.. (2019). Eco-Friendly Synthesis of Fe3O4 Nanoparticles Based on Natural Stabilizers and Their Antibacterial Applications. ChemistrySelect. 4. 10.1002/slct.201901594.
- 9. Ahadpour Shal, A. & Jafari, Atefeh. (2013). Study of Structural and Magnetic Properties of Superparamagnetic Fe3O4-ZnO Core-Shell Nanoparticles. Journal of Superconductivity and Novel Magnetism. 10.1007/s10948-013-2469-9.
- 10. Moeni, M., Edokali, M., Rogers, M. et al. (5 more authors) (2024) Effect of reaction and post-treatment conditions on physico-chemical properties of magnetic iron oxide nano-particles. Particuology, 91. pp. 155-167. ISSN 1674-2001
- 11. Kumar, Mukesh; Rany, Madhavi Ansari, Jamilur R. (2024) Chemical Methods for Producing Iron Oxide Magnetic Nanoparticles: A Review.
- 12. Hussein, Mohd & Suzariana, Samuri & Shaari, Abdul. (2013). The Effect of Synthesis Method on the Physico-Chemical Properties of Magnetite Iron Oxide Nanoparticles. Advanced Materials Research. 701. 212-216. 10.4028/www.scientific.net/AMR.701.212.
- 13. Yousif, Nwar & Aljawad, Selma & Taha, Ali & Stamatis, Haralambos. (2023). A Review of Structure, Properties, and Chemical Synthesis of Magnetite Nanoparticles. Journal of Applied Sciences and Nanotechnology. 3. 18-31. 10.53293/jasn.2022.5179.1178.
- 14. Khan, Nida & Jameel, Namra. (2023). Magnetic Nanoparticles-Synthesis, Properties and Potential Applications. 3.
- 15. Korsakova, Alina & Kotsikau, Dzmitry & Haiduk, Yulyan & Pankov, Vladimir. (2020). Synthesis and Physicochemical Properties of MnxFe3–xO4 Solid Solutions. Kondensirovannye sredy i mezhfaznye granitsy = Condensed Matter and Interphases.

- 16. 466-472. 10.17308/kcmf.2020.22/3076.
- 17. Che Soh, Siti & mohd yusof, Mohd & Abd Rahman Azmi, Alyza & Shamsuddin, Mustaffa & Wan Nor, Wan Fatihah. (2018). Synthesis and Physicochemical Properties of Magnetite Nanoparticles (Fe3O4) as Potential Solid Support for Homogeneous Catalysts. Malaysian Journal of Analytical Sciences. 22. 768-774. 10.17576/mjas-2018-2205-04.
- 18. Sabbas, N.P.. (2014). Magnetic nanoparticles: Synthesis, physicochemical properties and role in biomedicine.
- 19. Mazrouaa, Azza & Mohamed, Manal & Fekry, Mohamed. (2019). Physical and magnetic properties of iron oxide nanoparticles with different molar ratio of ferrous and ferric. Egyptian Journal of Petroleum. 28. 10.1016/j.ejpe.2019.02.002.
- 20. Belanova, Anna & Gavalas, Nikos & Makarenko, Yuriy & Belousova, Mariya & Soldatov, Alexander & Zolotukhin, Peter. (2018). Physicochemical Properties of Magnetic Nanoparticles: Implications for Biomedical Applications In Vitro and In Vivo. Oncology Research and Treatment. 41. 139-143. 10.1159/000485020.
- 21. Lazzarini, Andrea & Colaiezzi, R. & Passacantando, Maurizio & D'Orazio, Franco & Arrizza, L. & Ferella, Francesco & Crucianelli, Marcello. (2021). Investigation of physico-chemical and catalytic properties of the Coating Layer of Silica-Coated Iron Oxide Magnetic Nanoparticles. Journal of Physics and Chemistry of Solids. 153. 110003. 10.1016/j.jpcs.2021.110003.
- 22. Alvarado-Noguez, Margarita & Matias-Reyes, A. Eunice & Pérez-González, Mario & Tomás, Sergio & Aguilar, Claudia & Dominguez Pacheco, Arturo & Arenas-Alatorre, Jesús & Cruz-Orea, A. & Carbajal-Tinoco, Mauricio & Galot-Linaldi, Jairo & Estrada, Elizabet & Vega, Libia & Santoyo-Salazar, J.. (2023). Processing and Physicochemical Properties of Magnetite Nanoparticles Coated with Curcuma longa L. Extract. Materials. 3020. 10.3390/ma16083020.
- 23. Wang, S. & Zhou, Y.. (2015). Magnetic nanoparticles: Synthesis, physicochemical properties and role in biomedicine.
- 24. Shoudho, Kishan Nandi & Uddin, Shihab & Rumon, Md. Mahamudul Hasan & Shakil, Md Salman. (2024). Influence of Physicochemical Properties of Iron Oxide Nanoparticles on Their Antibacterial Activity. 10.1021/acsomega.4c02822.
- 25. Klekotka, Urszula & Satula, Dariusz & Spassov, Simo & Kalska-Szostko, Beata. (2017). Surfactant dependence on physicochemical properties of magnetite nanoparticles. Colloids and Surfaces A: Physicochemical and Engineering Aspects. 537. 10.1016/j.colsurfa.2017.10.054.
- 26. Soler, M.A.G. & Paterno, Leonardo. (2017). Magnetic Nanomaterials. 10.1016/B978-0-323-49782-4.00006-1.
- 27. Yadollahpour, Ali & Rashidi, Samaneh. (2015). Magnetic Nanoparticles: A Review of Chemical and Physical Characteristics Important in Medical Applications. Oriental Journal of Chemistry. 31. 25-30. 10.13005/ojc/31.Special-Issue1.03.
- 28. Radu, T. & Petran, Anca & Olteanu, Elena & Baldea, Ioana & Potara, Monica & Turcu, Rodica. (2019). Evaluation of physico-chemical properties and biocompatibility of new surface functionalized Fe3O4 clusters of nanoparticles. Applied Surface Science. 501. 144267. 10.1016/j.apsusc.2019.144267.

- 29. He, Yi & Yi, Chen & Zhang, Xiliu & Zhao, Wei & Yu, Dongsheng. (2021). Magnetic graphene oxide: Synthesis approaches, physicochemical characteristics, and biomedical applications. TrAC Trends in Analytical Chemistry. 136. 116191. 10.1016/j.trac.2021.116191.
- 30. Catalano, Enrico & Di Benedetto, Andrea. (2017). Characterization of physicochemical and colloidal properties of hydrogel chitosan-coated iron-oxide nanoparticles for cancer therapy. Journal of Physics: Conference Series. 841. 012010. 10.1088/1742-6596/841/1/012010.
- 31. Jungcharoen, Phoomipat & Marsac, Rémi & Choueikani, Fadi & Masson, Delphine & Pédrot, Mathieu. (2023). Influence of organic ligands on the stoichiometry of magnetite nanoparticles. Nanoscale Advances. 5. 10.1039/D3NA00240C.
- 32. Kabir, Hadi & Aghdam, M. & Samandari, Saeed & Moeini, Mohsen. (2024). A molecular dynamics study on the size effects of Fe 3 O 4 nanoparticles on the mechanical characteristics of polypyrrole/Fe 3 O 4 nanocomposite. Molecular Simulation. 50. 1-13. 10.1080/08927022.2024.2323200.
- 33. Falciglia, Pietro & Gagliano, Erica & Scandura, Pietro & Bianco, Carlo & Tosco, Tiziana & Sethi, Rajandrea & Varvaro, Gaspare & Agostinelli, Elisabetta & Bongiorno, Corrado & Russo, Antonio & Romano, Stefano & Malandrino, Graziella & Roccaro, Paolo & Vagliasindi, Federico. (2022). Physico-magnetic properties and dynamics of magnetite (Fe3O4) nanoparticles (MNPs) under the effect of permanent magnetic fields in contaminated water treatment applications. Separation and Purification Technology. 296. 121342. 10.1016/j.seppur.2022.121342.
- 34. Faraudo, Jordi & Andreu, Jordi & Calero, Carles & Camacho, Juan. (2016). Predicting the Self-Assembly of Superparamagnetic Colloids under Magnetic Fields. Advanced Functional Materials. 26. n/a-n/a. 10.1002/adfm.201504839.
- 35. Malatji, Nompumelelo & Makhado, Edwin & Modibane, Kwena & Ramohlola, Kabelo Edmond & Maponya, Thabiso & Monama, Gobeng & Hato, Mpitloane. (2021). Nanomaterials and Technologies for Environmental Applications -Review Article Removal of methylene blue from wastewater using hydrogel nanocomposites: A review. Nanomaterials and Nanotechnology. 11. 1-27. 10.1177/18479804211039425.
- 36. Myrovali, Eirini & Papadopoulos, Kyrillos & Iglesias, Irene & Spasova, Marina & Farle, Michael & Wiedwald, Ulf & Angelakeris, Makis. (2021). Long-Range Ordering Effects in Magnetic Nanoparticles. ACS applied materials & interfaces. 13. 10.1021/acsami.1c01820.
- 37. Ali, Arbab & Shah, Tufail & Ullah, Rehmat & Zhou, Pingfan & Guo, Manlin & Ovais, Muhammad & Tan, Zhiqiang & Yukui, Rui. (2021). Review on Recent Progress in Magnetic Nanoparticles: Synthesis, Characterization, and Diverse Applications. Frontiers in Chemistry. 9. 10.3389/fchem.2021.629054.
- 38. Wagh, Kalpeshkumar & Singh, (2023). Magnetic Nanoparticles as Advanced Drug Delivery Techniques for Breast Cancer: A Review. 8. 109-114.
- 39. Schwan, Jonas & Markert, Simon & Rosenfeldt, Sabine & Schüler, Dirk & Mickoleit, Frank & Schenk, Anna. (2023). Comparing the Colloidal Stabilities of Commercial and Biogenic Iron Oxide Nanoparticles That Have Potential In Vitro/In Vivo Applications. Molecules. 28. 4895. 10.3390/molecules28134895.

- 40. Bisla, Amarjeet & Honparkhe, Mrigank & Srivastava, Neeraj. (2022). A review on applications and toxicities of metallic nanoparticles in mammalian semen biology. Andrologia. 54. 10.1111/and.14589.
- 41. Kushwaha, Pratishtha & Chauhan, Pratima. (2022). A Simple One-Step Synthetic Approach for Preparation of α and γ -Fe 2 O 3 Nanoparticles: Studies of Structural and Magnetic Properties. Journal of Information and Computational Science. 357-366. 10.12733/JICS.2021.V11I1.535569.19639.
- 42. Mukhortova, Yu & Pryadko, Artyom & Chernozem, Roman & Pariy, Igor & Akoulina, Elizaveta & Demianova, Irina & Zharkova, I. & Ivanov, Yu & Wagner, Dmitry & Bonartsev, Anton & Surmenev, Roman & Surmeneva, M.. (2022). Fabrication and characterization of a magnetic biocomposite of magnetite nanoparticles and reduced graphene oxide for biomedical applications. Nano-Structures & Nano-Objects. 29. 100843. 10.1016/j.nanoso.2022.100843.
- 43. Sahadevan, Jhelai & Sojiya, R. & Padmanathan, N. & Kulathuraan, K. & Shalini, M.G. & Prakash, P.Siva & Muthu, Esakki. (2021). Magnetic property of Fe2O3 and Fe3O4 nanoparticle prepared by solvothermal process. Materials Today: Proceedings. 58. 10.1016/j.matpr.2021.11.420.
- 44. Crintea, Lenuța & Musat, Viorica & Silviu, Polosan & Ceoromila, Alina & Vasile, Basliu & Botezatu, Andreea-Veronica & Dinica, Rodica-Mihaela. (2020). Synthesis and characterization of magnetic oxide nanoparticles and corresponding thin films for wastewaters treatment. Ovidius University Annals of Chemistry. 31. 10.2478/auoc-2020-0021.
- 45. Hufschmid, Ryan & Landers, Joachim & Shasha, Carolyn & Salamon, Soma & Wende, Heiko & Krishnan, Kannan. (2018). Nanoscale Physical and Chemical Structure of Iron Oxide Nanoparticles for Magnetic Particle Imaging. physica status solidi (a). 216. 10.1002/pssa.201800544.
- 46. Ansari, Shoeb Anwar Mohammed Khawja, Eleonora Ficiarà, Federico Alessandro Ruffinatti, Ilaria Stura, Monica Argenziano, Ornella Abollino, Roberta Cavalli, Caterina Guiot, and Federico D'Agata. 2019. "Magnetic Iron Oxide Nanoparticles: Synthesis, Characterization and Functionalization for Biomedical Applications in the Central Nervous System" Materials 12, no. 3: 465. https://doi.org/10.3390/ma12030465
- 47. Gareev, Kamil & Grouzdev, Denis & Koziaeva, Veronika & Sitkov, Nikita & Gao, Huile & Zimina, Tatiana & Shevtsov, Maxim. (2022). Biomimetic Nanomaterials: Diversity, Technology, and Biomedical Applications. Nanomaterials. 12. 2485. 10.3390/nano12142485.
- 48. Mohammed, Ayad & Hashim, Ahmed. (2022). An Overview of Iron Oxide Nanoparticles: Characterisation, Synthesis, and Potential Applications. 20. 145-158.
- 49. Rajput, Shalini & Pittman, Charles & Mohan, Dinesh. (2015). Magnetic Magnetite (Fe3O4) Nanoparticle Synthesis and Applications for Lead (Pb2+) and Chromium (Cr6+) Removal from Water. Journal of Colloid and Interface Science. 468. 10.1016/j.jcis.2015.12.008.
- 50. Sajid, Muhammad & Shuja, Sidra & Rong, Hongpan & Zhang, Jiatao. (2023). Size-controlled synthesis of Fe3O4 and Fe3O4@SiO2 nanoparticles and their

- superparamagnetic properties tailoring. Progress in Natural Science: Materials International. 33. 10.1016/j.pnsc.2022.08.003.
- 51. Paut, Andrea & Guć, Lucija & Vrankić, Martina & Crnčević, Doris & Šenjug, Pavla & Pajić, Damir & Odžak, Renata & Sprung, Matilda & Nakić, Kristian & Marciuš, Marijan & Prkić, Ante & Mitar, Ivana. (2024). Plant-Mediated Synthesis of Magnetite Nanoparticles with Matricaria chamomilla Aqueous Extract. Nanomaterials. 14. 729. 10.3390/nano14080729.
- 52. Dilnawaz, Dr & Sahoo, Sanjeeb. (2022). Application of magnetic nanoparticles as drug delivery in cancer. 10.1016/B978-0-12-822819-7.00007-7.
- 53. Ananth, K. & Jose, Sujin & Kunga Sugumaran, VENKATESH & Rajangam, Ilangovan. (2013). Size Controlled Synthesis of Magnetite Nanoparticles Using Microwave Irradiation Method. Journal Nano Research. 24.
- 54. 10.4028/www.scientific.net/JNanoR.24.184.
- 55. Joudeh, N., Linke, D. Nanoparticle classification, physicochemical properties, characterization, and applications: a comprehensive review for biologists. J Nanobiotechnol 20, 262 (2022). https://doi.org/10.1186/s12951-022-01477-8
- 56. Stiufiuc, Gabriela Fabiola, and Rares Ionut Stiufiuc. 2024. "Magnetic Nanoparticles: Synthesis, Characterization, and Their Use in Biomedical Field" Applied Sciences 14, no. 4: 1623. https://doi.org/10.3390/app14041623
- 57. Wallyn J, Anton N, Vandamme TF. Synthesis, Principles, and Properties of Magnetite Nanoparticles for In Vivo Imaging Applications-A Review. Pharmaceutics. 2019 Nov 12;11(11):601. doi: 10.3390/pharmaceutics11110601. PMID: 31726769; PMCID: PMC6920893.
- 58. Sharma, A., Foppen, J.W., Banerjee, A. et al. Magnetic Nanoparticles to Unique DNA Tracers: Effect of Functionalization on Physico-chemical Properties. Nanoscale Res Lett 16, 24 (2021). https://doi.org/10.1186/s11671-021-03483-5
- 59. Ali A, Shah T, Ullah R, Zhou P, Guo M, Ovais M, Tan Z and Rui Y (2021) Review on Recent Progress in Magnetic Nanoparticles: Synthesis, Characterization, and Diverse Applications. Front. Chem. 9:629054. doi: 10.3389/fchem.2021.629054
- 60. Alina Mihaela Prodan, Simona Liliana Iconaru, Carmen Mariana Chifiriuc, Coralia Bleotu, Carmen Steluta Ciobanu, Mikael Motelica-Heino, Stanislas Sizaret, Daniela Predoi(2013) Magnetic Properties and Biological Activity Evaluation of Iron Oxide Nanoparticles.
- 61. Ali A, Zafar H, Zia M, ul Haq I, Phull AR, Ali JS, Hussain A. Synthesis, characterization, applications, and challenges of iron oxide nanoparticles. Nanotechnol Sci Appl. 2016;9:49-67
- 62. Nguyen, M.D.; Tran, H.-V.; Xu, S.; Lee, T.R. Fe3O4 Nanoparticles: Structures, Synthesis, Magnetic Properties, Surface Functionalization, and Emerging Applications. Appl. Sci. 2021, 11, 11301. https://doi.org/10.3390/app112311301
- 63. Aakanksha Arvind Pati (2021) Nanoparticles: Properties, Applications and Toxicities.
- 64. Nene Ajinkya, Xuefeng Yu, Poonam Kaithal, Hongrong Luo, Prakash Somani and Seeram Ramakrishna (2020) Magnetic Iron Oxide Nanoparticle (IONP) Synthesis to Applications: Present and Future.
- 65. Sahar IA Al-Baldawi, Anes IS Al-Sammarraie, Firas H Alwade, Preparation and

- Characterization Iron Oxide (Fe3O4) Magnetic Nano Particleg, J Res Med Dent Sci, 2019, 7(6): 107-112.
- 66. J.H. Koo, Polymer Nanocomposites, The McGraw Hills Companies, New York, 2006, pp. 2–4.
- 67. G D'Costa, DS Pisal, AV Rane; Report on Synthesis of nanoparticles and functionalization: Coprecipitation method, 2012.
- 68. S Patankar, D Magdum, P Patil, S Pakhale; Report on Synthesis of nanoparticles using ion sputtering method, 2012.
- 69. V. Chikan, E.J. McLaurin, Rapid nanoparticle synthesis by magnetic and microwave heating, Nanomaterials 6 (2016) 85, https://doi.org/10.3390/nano6050085.
- 70. R Jain, SK Chaurasia, A Kalga; Report on Sol gel method for nanoparticle synthesis, 2012.
- 71. A.A. Efimov, A.A. Lizunova, I.A. Volkov, D.A. Mylnikov, P.V. Arsenov, V.V. Ivanov, A new approach to the high-yield synthesis of nanoparticles by spark discharge, J. Phys. Conf. Ser. 741 (2016) (2016), https://doi.org/10.1088/1742-6596/741/1/012035.
- 72. N. Pantidos, L.E. Horsfall, Biological synthesis of metallic nanoparticles by bacteria, fungi and plants, J. Nanomed. Nanotechnol. 5 (2014) 233, https://doi.org/10.4172/2157-7439.1000233.
- 73. P.H.C. Camargo, K.G. Satyanarayana, F. Wypych, Nanocomposites: synthesis, structure, properties and new application opportunities, Mater. Res. 12 (1) (2009) 1–39.
- 74. Y.H. Choa, J.K. Yang, B.H. Kim, Y.K. Jeong, J.S. Lee, T. Nakayama, et al., Preparation and characterization of metal: ceramic nanoporous nanocomposite powders, J. Magn. Magn. Mater. 266 (1–2) (2003) 12–19